small
NANO MICRO

Epidermal Growth Factor–Ferritin H-Chain Protein Nanoparticles for Tumor Active Targeting

Xu Li, Lihui Qiu, Pei Zhu, Xinyi Tao, Tadayuki Imanaka, Jing Zhao, Youguo Huang, Yaping Tu, and Xuni Cao**

***H**uman ferritin H-chain protein (FTH1)-based nanoparticles possess a precisely assembled nanometer-scale structure and high safety. However, their applications for imaging and drug delivery towards cancer cells remain limited due to a lack of target specificity. Epidermal growth factor receptor (EGFR) is overexpressed in many malignant tissues including breast cancer, and has been used as a therapeutic target for cancer treatment. Herein, a genetic method is shown to generate EGF-FTH1 chimeric proteins. EGF-FTH1 nanoparticles with EGF on the surface are then produced. The data demonstrate that EGF-FTH1 nanoparticles, with a small size (11.8 ± 1.8 nm), narrow size distribution, and high biosafety, can specifically bind to and then be taken up by breast cancer MCF-7 cells and MDA-MB-231 cells, but not normal breast epithelial MCF-10A cells. In contrast, binding and absorption of nontargeted ferritin-based nanoparticles to breast cancer cells are negligible. In vivo studies show that EGF-FTH1 nanoparticles are accumulated in breast tumors in a mouse xenograft model. Interestingly, the concentration of EGF-FTH1 nanoparticles in the tumor site is significantly reduced when mice are pretreated with an excess of free EGF. These results imply that EGF–EGFR interaction plays an important role in regulating the tumor retention of EGF-FTH1 nanoparticles.*

1. Introduction

Cancer remains one of the leading causes of death in the world. Despite advances in our understanding of cancer biology and the development of novel approaches permitting earlier detection, the overall survival rate from advanced cancer has not significantly improved in the past two decades.[1] Thus, there is an urgent need for new methods to selectively target cancer cells for destruction by chemotherapy.

Recent advances in nanoscience and nanotechnology have led to the development of nanomaterials for cancer detection and treatment.[2,3] Spherical protein cages can be viewed as precisely assembled nanometer-scale containers. In nature, viral capsids, ferritins, and some heat shock proteins self-assemble from multiple copies of protein subunits to form protein cages.[4,5] For example, ferritins are composed of 24 subunits to form cage architectures 12 nm in diameter with an interior cavity 8 nm in diameter. Mammalian ferritin consists

X. Li, L. Qiu, P. Zhu, X. Tao, Prof. T. Imanaka, Prof. X. Cao
State Key Laboratory of Bioreactor Engineering
East China University of Science & Technology
Shanghai 200237, China
E-mail: caoxuni@ecust.edu.cn
Prof. Y. Tu
Department of Pharmacology
Creighton University
School of Medicine
Omaha, NE 68178, USA
E-mail: YapingTu@creighton.edu
J. Zhao, Prof. Y. Huang
National Laboratory of Biomacromolecules
Institute of Biophysics
Chinese Academy of Sciences
Beijing 100101, China

DOI: 10.1002/smll.201200066

of a mixture of two different types of subunits known as heavy (H) and light (L) chains. Recombinant ferritin H-chain proteins (FTH1) show a well-assembled architecture and the same iron storage activity as the natural copolymer of human ferritin.[6,7] FTH1-based nanoparticles are suitable for cancer imaging or treatment because: 1) these protein nanoparticles have higher biosafety than other nanoscale therapeutic delivery systems such as silica nanoparticles, dendrimer-based nanoparticles, or metal-based nanoparticles;[5] 2) they are less immunogenic than virus-based protein cages;[8] and 3) most importantly, FTH1 nanoparticles are highly amenable to both genetic and chemical modifications without altering the assembly and overall architecture of the cage.[9]

Several groups have demonstrated the ability to simultaneously impart multiple functionalities to a single protein cage, by utilizing a chemical means of modification and genetic engineering.[10–12] Antibodies, folic acid, and RGD-4C peptide have been reported to be incorporated into protein cages.[9,13–15] These nanoparticles might be a very promising delivery system for targeting human cancer. However, it is still a matter of debate whether functionalization with homing ligands is able to guide nanoparticles to tumors by active targeting, or nanoparticle delivery is rather mediated by passive transport. Chen et al. reported that RGD peptide-functionalized ferritin nanocages can accumulate in the tumor due to both RGD-integrin targeting and the enhanced permeability and retention (EPR) effect. They showed nanoparticles were more susceptible to washout and lymphatic drainage without RGD-integrin interaction. It seemed that RGD-integrin targeting would not increase accumulation of nanoparticles in tumors.[16] However, so far it is not clear about the in vivo behavior of other targeted ferritin-based nanoparticles, especially whether active targeting would guide nanoparticles to tumor sites. That is, the targeting mechanism of ferritin-based nanoparticles still needs to be examined.

Herein, genetic engineering represents a much easier and more reproducible method of generating protein-based nanoparticles with exactly the same architecture as those obtained with chemical modifications. Thus, we explored the possibility of coupling FTH1 nanoparticles with probe molecules for tumor targeting. The epidermal growth factor (EGF) receptor (EGFR) signaling pathway plays an important role in the regulation of cell proliferation, survival, and differentiation.[17] Upregulation of EGFR is found in many types of cancer and has already provided a rationale for designing receptor-targeted approaches used for both cancer imaging and treatment.[18] EGF is the EGFR ligand and can be used as a probe molecule. Moreover, the fact that EGF–EGFR complexes are internalized by cells led us to postulate that FTH1 nanoparticles with EGF on their surfaces could provide a method for targeted intracellular delivery of chemotherapeutic drugs by these nanoparticles. We first used genetic methods to prepare EGF-FTH1 nanoparticles. After testing the biosafety of the generated nanoparticles, we carefully investigated the ability of EGF-FTH1 nanoparticles to target breast cancer cells in vitro and tumors in vivo. We found that the EGF–EGFR interaction played an important role in the accumulation of nanoparticles in tumors. Altogether, our data demonstrate that EGF-FTH1 nanoparticles might be very promising for clinical applications. Moreover, a similar strategy could be applied to generate other protein-based nanoparticles with surface-attached polypeptides in an efficient and reliable manner suitable for industrial production.

2. Results

2.1. Development and Characterization of EGF-FTH1 Nanoparticles

To develop EGF-FTH1 nanoparticles, EGF was first genetically fused to the N terminus of FTH1 protein, and the fusion protein was expressed in *Escherichia coli* BL21(DE3) cells. As shown in **Figure 1**A, isopropyl-β-D-thiogalactoside (IPTG) induced high expression of EGF-FTH1 protein, but a majority of the EGF-FTH1 fusion protein was insoluble

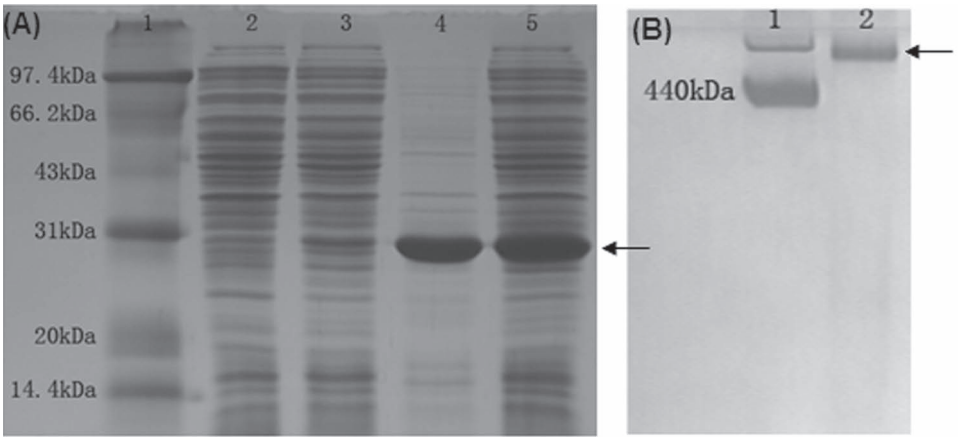

Figure 1. Expression and purification of EGF-FTH1 in *E. coli*. BL21(DE3). A) Solubility of EGF-FTH1 in *E. coli*. BL21(DE3) analyzed by 10% SDS-PAGE and stained with Coomassie blue. Lane 1, molecular marker; lane 2, the whole cell lysate without IPTG induction (8 μg); lane 3, soluble fraction of EGF-FTH1 overexpressed in *E. Coil* with 1 mM IPTG induction (8 μg); lane 4, insoluble fraction of EGF-FTH1 overexpressed in *E. coil* with 1 mM IPTG induction; lane 5, total cell lysates with 1 mM IPTG induction. B) Recombinant EGF-FTH1 was analyzed by 7% native PAGE and stained with Coomassie blue. Line 1: apoferritin from equine spleen (Sigma, 8 μg); line 2, EGF-FTH1 (8 μg).

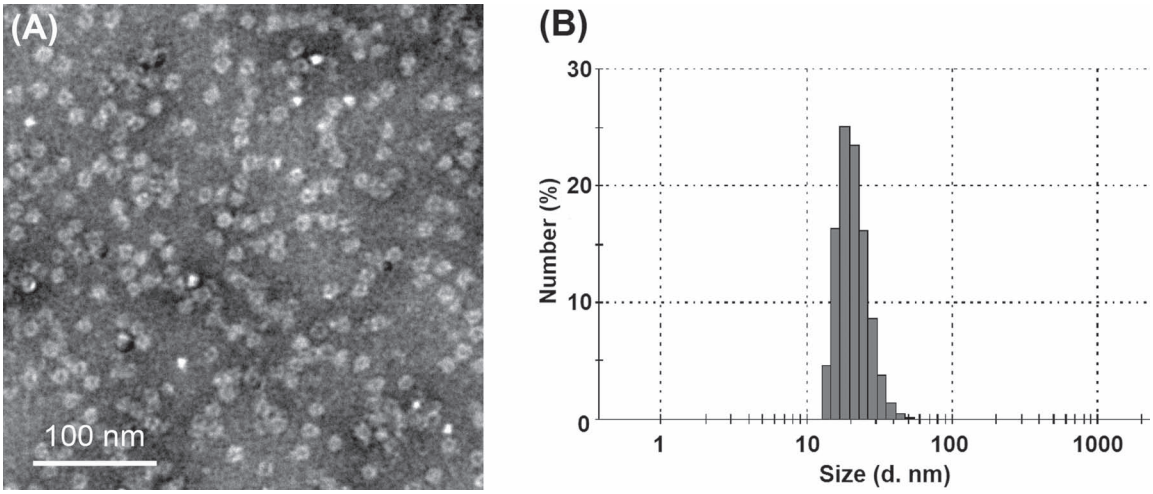

Figure 2. TEM image and DLS analysis of EGF-FTH1 nanoparticles. A) Typical TEM image of EGF-FTH1 nanoparticles observed with 1% phosphotungstic acid staining. EGF-FTH1 nanoparticles are approximately 12 nm in diameter. B) DLS analysis shows they are 19 nm in solution.

in the cytoplasm. Alterations of the IPTG induction conditions did not improve EGF-FTH1 fusion protein solubility (data not shown). Therefore, the insoluble macroaggregates of EGF-FTH1 were solubilized in buffer containing 8 M urea. The urea was removed by a stepwise dialysis procedure, which resulted in EGF-FTH1 proteins that were refolded into active form. Native sodium dodecyl sulfate–polyacrylamide gel electrophoresis (SDS-PAGE) results showed a protein with a molecular weight (MW) of 672 kD indicating that these proteins had self-assembled into the apoferritin structure (Figure 1B).

EGF-FTH1 nanoparticles were further analyzed by transmission electron microscopy (TEM), which revealed that EGF-FTH1 adopted the expected spherical cagelike structure with a diameter of 11.8 ± 1.8 nm (**Figure 2**A). There was no significant difference between EGF-FTH1 nanoparticles and FTH1 or apoferritin nanoparticles (data not shown). Dynamic light scattering (DLS) results also confirmed that EGF-FTH1 nanoparticles were very stable and monodispersed in solution with a size of 19.0 ± 1.2 nm, which is the hydrodynamic diameter of EGF-FTH1 (Figure 2B). All these results indicated that fusion of EGF to the N terminus of the FTH1 subunit did not interfere with the self-assembly of the subunits to form the characteristic 24-subunit protein cage architecture of apoferritin.

2.2. Evaluation of the Biosafety of EGF-FTH1 Nanoparticles In vitro and In vivo

We further investigated the cytotoxicity of EGF-FTH1 nanoparticles. Normal breast epithelia MCF-10A cells, breast cancer MCF-7 cells, and MDA-MB-231 cells were treated with EGF, apoferritin, or EGF-FTH1 nanoparticles in full growth medium for 48 h. As shown in **Figure 3**A, MTT assay revealed that neither 20 ng μL^{-1} of EGF nor 6 μM of apoferritin had any significant effect on the viability of MCF-7 and MDA-MB-231 cells when compared to untreated controls. More importantly, 6 μM EGF-FTH1 nanoparticles also had no effect on cell viability in these cell lines.

Next we assessed the toxicity of EGF-FTH1 nanoparticles in vivo by analyzing their effect on body weight change and tumor growth using nude mice bearing MDA-MB-231 tumor xenografts. When the tumor volume reached approximately 100 mm^3, EGF-FTH1 nanoparticles (1.0 nmol) were injected into mice every other day for 10 days. During the dosing period the body weight and tumor size were measured every day. As shown in Figure 3B, the EGF-FTH1 nanoparticle groups did not experience any acute depression in body weight in these 10 days when compared to PBS control groups. In addition, EGF-FTH1 nanoparticles (1.0 nmol) had no stimulatory effect on tumor growth (Figure 3C). Thus, EGF-FTH1 nanoparticles are probably safe enough for cancer-cell imaging and drug-delivery applications.

2.3. EGF Units Required for Binding of EGF-FTH1 Nanoparticles to MCF-7 Cells

To test the cell binding ability of EGF-FTH1 nanoparticles, fluorescence-activated cell sorting (FACS) analysis was performed using fluorescein-labeled nanoparticles. Native PAGE showed successful fluorescein labeling of EGF-FTH1 nanoparticles (shown in **Figure 4**), and the number of conjugated fluorescein molecules was determined by absorbance spectroscopy to be 7.92 per cage for EGF-FTH1. The same procedures were carried out for apoferritin; the number of fluorescein molecules per apoferritin molecule was 4.8. **Figure 5**A shows a typical FACS analysis of binding of fluorescein-labeled EGF-FTH1 nanoparticles to MCF-7 breast cancer cells that express endogenous EGFR. MCF-7 cells had very low autofluorescence with a geometric mean fluorescence intensity value of 3.63. However, after incubation with various concentrations of fluorescein-labeled EGF-FTH1 nanoparticles, the geometric mean fluorescence intensity value of the cells increased in a nanoparticle-dose-dependent manner

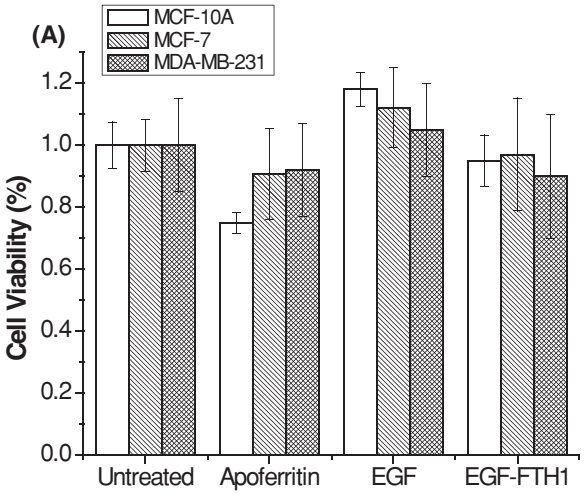

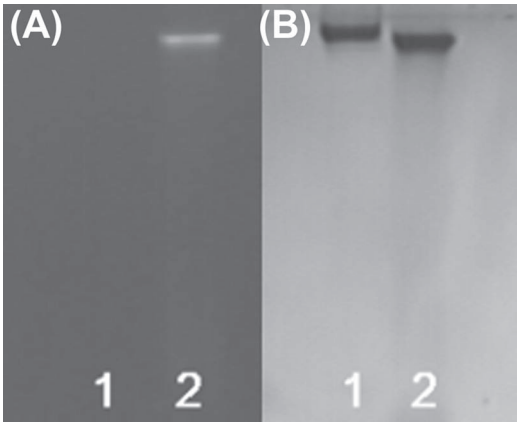

Figure 4. Confirmation of EGF-FTH1 conjugate by 7% native PAGE using A) fluorescence detection or B) staining with Coomassie blue. Lane 1, EGF-FTH1 nanoparticles (8 μg); lane 2, fluorescein-labeled EGF-FTH1 nanoparticles (8 μg).

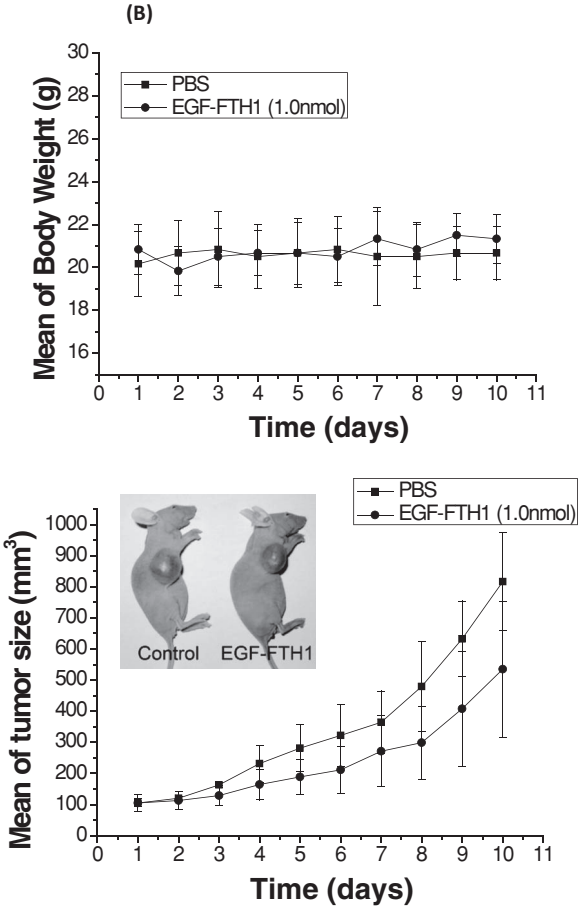

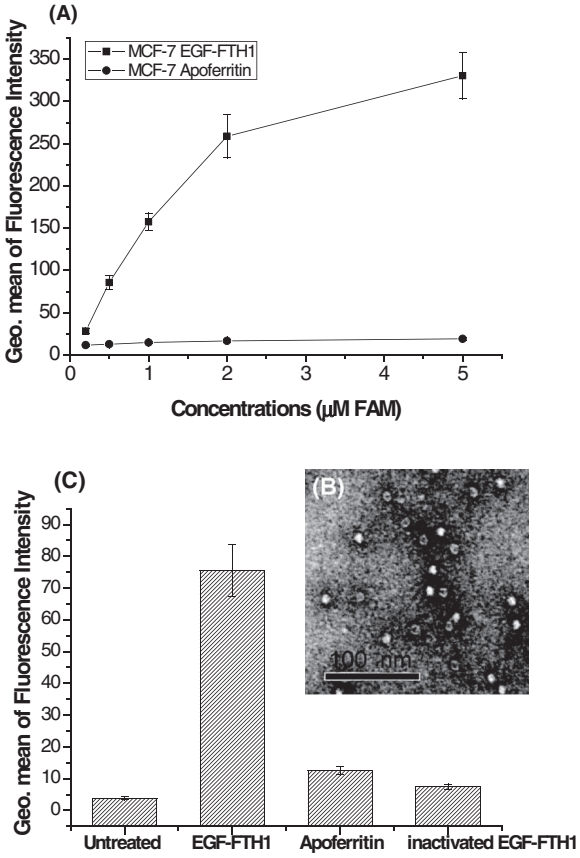

Figure 3. Analysis of the biosafety of EGF-FTH1 nanoparticles. A) Cell viability of EGF, apoferritin, and EGF-FTH1 nanoparticles; 1×10^3 MCF-10A cells, 3×10^3 MCF-7 cells, and 3×10^3 MDA-MB-231 cells were incubated with EGF (20 ng mL^{-1}), apoferritin (6 μM), and EGF-FTH1 (6 μM) for 48 h and then analyzed by MTT assay. Data represent the mean ± standard deviation (SD), $n = 4$. B) In vivo biosafety assay of EGF-FTH1 nanoparticles. Body weight change (top) and tumor size (bottom) as a function of time in nude mice bearing MDA-MB-231 tumor xenografts with intravenous (i.v.) tail-vein injections of either phosphate-buffered saline (PBS) (■) or 1.0 nmol EGF-FTH1 nanoparticles (●) every other day for 10 days (data represent mean ± SD, $n = 3$). The inset shows there was no significant difference between tumor-bearing mice treated with EGF-FTH1 nanoparticles and PBS.

Figure 5. Binding of cages to MCF-7 cells measured by FACS. A) 5×10^5 MCF-7 cells were incubated with different concentrations of fluorescein-labeled EGF-FTH1 nanoparticles (■) and apoferritin nanoparticles (●) at 4 °C for 1 h. The concentrations of cages are indicated as the concentrations of fluorescein conjugated to the cages. The increased level of fluorescence intensity of the cells indicates efficient binding of EGF-FTH1 to MCF-7 cells. Data represent mean ± SD, $n = 3$. B) TEM image of inactivated EGF-FTH1 nanoparticles, which indicates they are well assembled. C) 5×10^5 MCF-7 cells were incubated with fluorescein-labeled nanoparticles at 4 °C for 1 h. Nanoparticles were normalized to 0.5 μM fluorescein. The decreased level of fluorescence intensity for inactivated EGF-FTH1 nanoparticles indicates their extremely weak binding to the MCF-7 cells. Data represent mean ± SD, $n = 3$.

NANO MICRO small

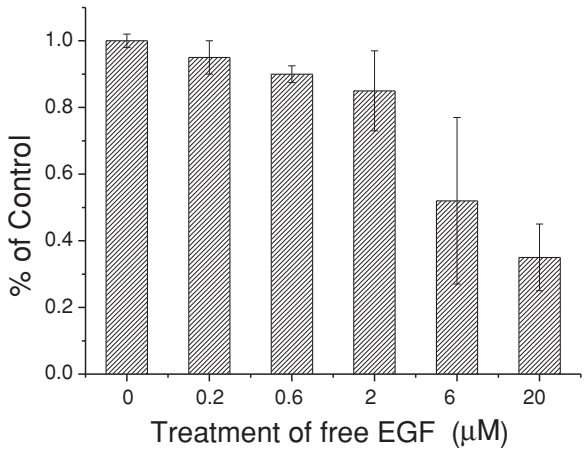

Figure 6. Competition of EGF-FTH1 nanoparticles bonded to MCF-7 using free EGF. FACS analysis of 5×10^5 MCF-7 cells incubated with fluorescein-labeled EGF-FTH1 (63 nM; 0.5 μM fluorescein-5-maleimide (FAM)) in the presence of increasing amounts of free EGF as indicated at 4 °C for 1 h. The decreased level of fluorescence intensity of the cells treated with free EGF indicates specific binding of EGF-FTH1 nanoparticles to EGFR expressed on the surface of the MCF-7 cells. Data represent the mean ± SD, $n = 3$.

with an EC_{50} of 152 ± 62 nM and a maximum geometric mean fluorescence intensity of 353.7 (Figure 5A). In contrast, cells incubated with flurorescein-labeled nontargeted apoferritin nanoparticles showed no significant increase in fluorescence intensities. This result suggested that EGF-FTH1 nanoparticles, but not apoferritin nanoparticles, were strongly associated with MCF-7 cells. Furthermore, we tested the binding ability of inactivated EGF-FTH1 nanoparticles to MCF-7 cells. Here, EGF-FTH1 nanoparticles were inactivated by employing pH induction. Generally, apoferritin would disassemble at pH 2 and reassemble into a protein cage structure when the pH of the solution increases to pH 7.[19] In this case, EGF-FTH1 protein can form the spherical cages after changing the pH (TEM data shown in Figure 5B), but the EGF units on the surface of the spherical EGF-FTH1 nanoparticles would not function well. As shown in Figure 5C, the inactivated EGF-FTH1 nanoparticles lost their binding ability towards MCF-7 cells. All these results meant that targeted units were required for ferritin-based nanoparticles to bind to MCF-7 cells.

To further demonstrate that the association of EGF-FTH1 nanoparticles with MCF-7 cells was dependent on EGF units on the surface of nanoparticles, competition experiments were performed. As shown in **Figure 6**, treatment of cells with free EGF attenuated association of EGF-FTH1 nanoparticles with MCF-7 cells in a concentration-dependent manner, thus suggesting that association of EGF-FTH1 with MCF-7 cells depended on interaction of EGF with EGFR of MCF-7 cells, and blocking EGFR with free EGF would lead to dissociation of EGF-FTH1 nanoparticles from the cells. In addition, free EGF attenuated association of EGF-FTH1 nanoparticles with MCF-7 cells with 65% reduction at 20 μM free EGF, whereas total EGF on EGF-FTH1 nanoparticles was about 1.52 μM. In this case, if each EGF unit on EGF-FTH1 acted as a free EGF molecule and each nanoparticle–cell contact was made by a single EGF–EGFR interaction, the IC_{50} value would, by definition, be equal to the nanoparticle-displayed EGF concentration of 1.52 μM. Thus, EGF displayed on the surface of a nanoparticle bonded with similar affinity on a per-EGF basis. As a matter of fact, on a per-nanoparticle basis the avidity of EGF-FTH1 for MCF-7 is much stronger than that of free EGF.

2.4. Targeting of EGF-FTH1 Nanoparticles to Breast Cancer Cells

To investigate the targeting ability towards cancer cells, we compared the association and subcellular distribution of fluorescein-labeled EGF-FTH1 nanoparticles with normal breast epithelia MCF-10A cells, breast cancer MCF-7 cells, and MDA-MB-231 cells. MCF-10A cells express an extremely low level of EGFR, MCF-7 cells express modest levels of EGFR, whereas MDA-MB-231 cells express a high level of EGFR.[20]

Association and subcellular distribution of EGF-FTH1 were analyzed after 3 h of incubation with these cells by using fluorescence microscopy. As shown in **Figure 7**, EGF-FTH1 nanoparticles but not apoferritin nanoparticles were transported into the cytosol of breast cancer MCF-7 and MDA-MB-231 cells. Treatment of cells with a high concentration of EGF (20 μM) largely blocked the cytoplasmic uptake of EGF-FTH1. As expected, much fewer EGF-FTH1 nanoparticles were found in the cytosol of MCF-10A cells when compared to that of MDA-MB-231 and MCF-7 cells. Together, these results suggested that EGF-FTH1 cytoplasmic uptake was dependent on EGFR binding and subsequent receptor-mediated endocytosis, and that the upregulated EGFR expression played a critical role in cytoplasmic uptake of EGF-FTH1 nanoparticles. Thus, EGF-FTH1 nanoparticles could not only be used for imaging, but also for the selective delivery of drugs since more of the drug would be selectively transported into the cancer cells.

2.5. Accumulation of EGF-FTH1 Nanoparticles in Breast Tumors In Vivo

To examine the tumor-targeting ability of EGF-FTH1 in vivo, Alexa Fluor 750 dye-labeled EGF-FTH1 nanoparticles were administered to mice bearing EGFR-positive MDA-MB-231 tumor xenografts. Two hours later, we analyzed the topographic distribution of EGF-FTH1 nanoparticles in mice by applying near-infrared fluorescence (NIRF) imaging. As shown in **Figure 8**A, high fluorescence intensities were detected in the tumor region (the area that the arrow points to). Such a high tumor accumulation could be caused by EGF–EGFR interaction and the EPR effect. To address this, another group of mice were injected with EGF (0.2 mg per mouse) 30 min prior to injection of Alexa Fluor 750 dye-labeled EGF-FTH1 nanoparticles. This preinjection of EGF largely blocked fluorescence accumulation in tumor regions. This observation confirmed that EGF–EGFR interaction

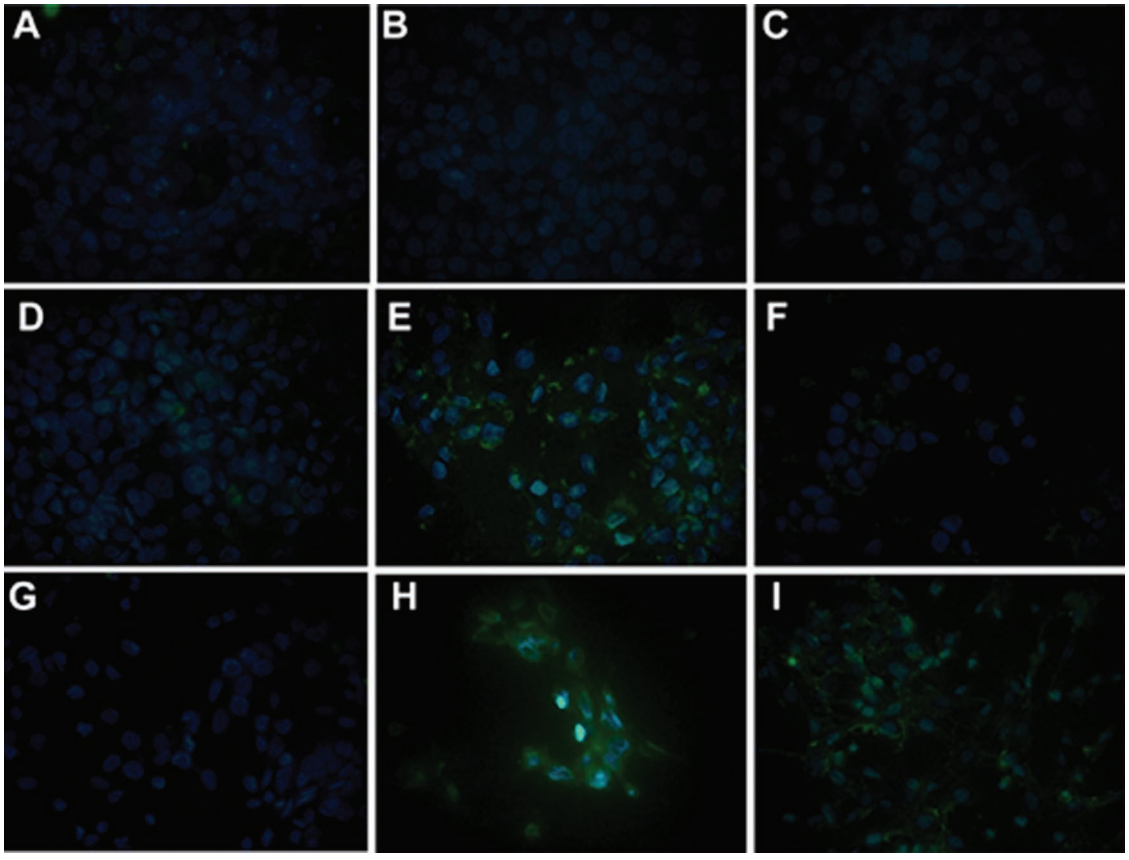

Figure 7. Typical fluorescence microscopic images of ferritin-based nanoparticles for targeting A–C) MCF-10A cells, D–F) MCF-7 cells, and G–I) MDA-MB-231 cells. 2.2×10^5 cells were incubated with fluorescein-labeled apoferritin nanoparticles (A, D, G) or fluorescein-labeled EGF-FTH1 nanoparticles without (B, E, H) or with treatment of cells with 20 μM EGF (C, F, I). Cells were imaged 3 h after incubation. (Nanoparticles were normalized to 0.5 μM fluorescein.)

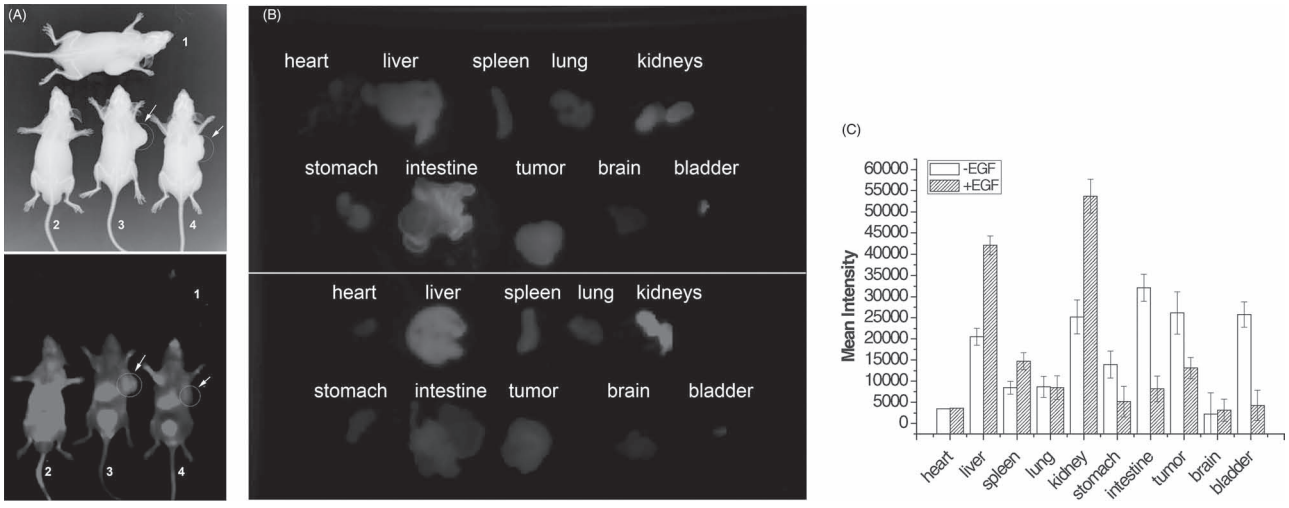

Figure 8. In vivo NIRF images of EGF-FTH1 nanoparticles. A) In vivo X-ray image (top) and NIRF image (bottom) of Balb/c athymic nude mice bearing a subcutaneous MDA-MB-231 xenograft tumor (3, 4) after intravenous injection of EGF-FTH1 nanoparticles (100 μL, 5 μM) conjugated with Alexa Fluor 750 without (3) or with pretreatment (4) by EGF (0.2 mg, 100 μL). Balb/c athymic nude mice injected with PBS and EGF-FTH1 nanoparticles conjugated with Alexa Fluor 750 were used as negative control (1) and positive control (2), respectively. The images were taken 2 h after the administration of EGF-FTH1 nanoparticles. The tumor location is specified with white arrows. B) Ex vivo NIRF images of major organs and tumors collected 2 h post-injection of EGF-FTH1 nanoparticles without (top) or with pretreatment by EGF (bottom). C) Quantification of the ex vivo tumor targeting characteristics of EGF-FTH1 in tumor-bearing mice. Data represent the mean ± SD, $n = 3$.

NANO MICRO small

contributed to the increased tumor accumulation of EGF-FTH1 nanoparticles. After that, mice were sacrificed and their tumors along with major organs were collected for ex vivo NIRF imaging (shown in Figure 8B). In accordance with the in vivo observation, a significant difference in tumor uptake was observed between the EGF blocking and nonblocking groups. By drawing three-dimensional regions of interest in the tumor and determining the fluorescence intensities, we found that pretreatment of EGF led to a 50% decrease in tumor accumulation of EGF-FTH1 nanoparticles. When the tissues were lysed with RIPA buffer and the fluorescence intensity was further measured, we were able to quantify the nanoparticles in the tumor, which were 3.1 ± 1.5 and 1.7 ± 1.1% ID g^{-1} ($n = 3$) for the nonblocking and blocking groups, respectively. Besides the high tumor accumulation of the nanoparticles, a great deal of fluorescence intensity was also detected in liver and kidney, similar to a previous report.[16] All together, our observation suggests that EGF–EGFR targeting plays an important role in regulating the tumor retention of EGF-FTH1 nanoparticles.

3. Discussion

Herein, we have shown a simple way to generate targeted EGF-FTH1 nanoparticles. It has been reported that various human proteins, including EGF, are soluble when they are fused to the C terminus of FTH1 and expressed in *E. coli* cells.[7] However, the EGF domain is not located on the surface of the spherical shell of the supramolecule.[7] Thus, we first fused EGF to the N terminus of the FTH1 to make a chemical construct. When this EGF-FTH1 fused protein was expressed in *E. coli* cells, it formed insoluble aggregates and could not form a spherical shell of the supramolecule in *E. coli* cytosol. This may be due to the reducing environment of bacterial cytosol that inhibits the formation of disulfide bonds of EGF units and easily leads to formation of protein aggregates.[21] So the EGF-FTH1 insoluble aggregates were recovered, and denatured by using 8 M urea. The denatured proteins were refolded into the active form by using traditional step dialysis. Importantly, this method also allowed EGF-FTH1 to form functional ferritin cages with EGF on the surface of the supramolecule. This approach is simple and can also be applied to other protein cages.

The resulting EGF-FTH1 nanoparticles show good targeting towards breast cancer MCF-7 cells and MDA-MB-231 cells as compared to normal breast epithelia MCF-10A cells. Although transferritin receptor-1 is highly expressed in many cell lines and some reports show ferritin-based nanoparticles could bind to these receptors,[19,22,23] our studies provide evidence indicating that association of EGF-FTH1 with breast cancer cells is dependent on EGFR but not transferritin receptor-1. For example, FACS analysis revealed that EGF-FTH1 nanoparticles, but not apoferritin nanoparticles or inactivated EGF-FTH1 nanoparticles, were associated with MCF-7 and MDA-MB-231 cells. In addition, free EGF attenuated association of EGF-FTH1 nanoparticles with EGFR-positive cells. Besides the specificity of EGF-FTH1 nanoparticles, their binding affinity to breast cancer cells is also very high. Generally, MCF-7 cells express modest levels of EGFR (≈10^4 receptors per cell).[24] Some groups reported that anti-EGFR antibody-conjugated nanoparticles, such as EGFR-targeted immunoliposomes,[24] scFv EGFR–quantum dots, scFv EGFR–magnetic iron oxide nanoparticles,[25] and anti-EGFR/gold nanoparticles,[26] did not efficiently target MCF-7 cells. However, we found that our EGF-FTH1 nanoparticles could efficiently bind to this cell line. Compared with nontargeted nanoparticles (apoferritin), the fluorescence intensity increased more than tenfold when these cells were incubated with fluorescein-labeled EGF-FTH1 nanoparticles. This association was so strong that it could only be disrupted by treatment with a high concentration of free EGF (>20 μM). The simplest explanation is that potentially multivalent EGF-FTH1 nanoparticle–cell surface interactions are of higher affinity than the single EGF–EGFR interaction. For example, there are 24 copies of EGF incorporated onto the surface of one nanoparticle and some of them can interact with one cell simultaneously, thereby enhancing the binding affinity.[27,28] This might be very important for delivering imaging/therapeutic agents to an EGFR-positive tumor in vivo.

We also observed internalization of EGF-FTH1 nanoparticles into MCF-7 and MDA-MB-231 cells. This is very important to develop a protein-based drug-delivery system because most native proteins cannot efficiently enter into cells. Our study indicated that EGF-FTH1 nanoparticles with small EGF ligand could easily enter into the cells via receptor-mediated endocytosis, but nontargeted apoferritin nanoparticles failed to do so. It seems that ferritin-based nanoparticles are quite different from other nanoparticles, such as polymer-based nanoparticles. Generally, polymer-based nanoparticles can be taken up by cells through endocytosis, which usually leads to higher nonspecific uptake. In contrast, uptake of nontargeted ferritin-based nanoparticles is negligible unless the receptor-targeting entities are available on the surface of the nanoparticles. Park and co-workers recently demonstrated that anti-HER2-scFv immunoliposomes achieved intracellular drug delivery via antibody-mediated endocytosis, thus leading to superior antitumor activity.[29] It is the internalization, rather than increased uptake in tumor tissue, that is responsible for the improved therapeutic output. Thus, EGF-dependent targeting may be a good choice for ferritin-cage-based nanoparticles to deliver active therapeutic agents into cancer cells.

Like most virus-based nanoparticles, we found that EGF-FTH1 nanoparticles could be delivered to the liver and kidney within the first 2 h.[30] However, these nanoparticles were not removed from the circulation so quickly. Thus, it favored their accumulation in tumors. Our preliminary data showed that tumor accumulation was evidenced for EGF-FTH1 nanoparticles, and this accumulation could be largely blocked by pretreatment with free EGF. It means that EGF–EGFR interaction plays an important role in this accumulation. However, such a difference in accumulation (3.1 ± 1.5 and 1.7 ± 1.1% ID g^{-1}) may not be significant in the context of overwhelming reticuloendothelial system (RES) uptake and passive targeting (EPR) in both groups. Thus, EGF-FTH1 nanoparticles can accumulate in the tumor site by a combination of passive and active targeting mechanisms.

Usually, active targeting has a marginal impact on nanoparticle accumulation or biodistribution in mouse xenograft models, whereas such targeting does provide greater intracellular delivery of therapeutic agents to cancer cells within solid tumors.[31,32] Therefore, we will further investigate the distribution of the EGF-FTH1 nanoparticles within the tumors in the future. Finally, in vivo evaluation of the biosafety of EGF-FTH1 nanoparticles showed that they would not stimulate the growth of the tumor although EGF ligands were on the surface of the nanoparticles. Thus, EGF-FTH1 nanoparticles are very promising for clinical applications.

4. Conclusion

EGF-FTH1 nanoparticles have been prepared as an example by using a genetic method. This method can also be used to incorporate some peptides, which might be insoluble in *E. coli* cytoplasm, onto the exterior surface of the ferritin H-chain protein. The method is very simple and is low-cost, and thus might be applied to industrial production. The EGF-FTH1 nanoparticles generated here show a precisely assembled nanometer-scale structure, and small size with narrow size distribution. The nanoparticles can be specifically taken up by EGFR-positive breast cancer cells depending on the targeted EGF units on the surface of the nanoparticles. In addition, these nanoparticles demonstrate a reasonable biosafety and in vivo tumor accumulation. Therefore, they are very promising for clinical applications.

5. Experimental Section

Materials and Reagents: The human FTH1 cDNA clone of MGC:5580 IMAGE:3459353 was obtained from Open Biosystems (BC000857). EcoR I, Not I, and Nco I restriction enzymes were purchased from New England Biolabs (Beijing). Takara Ex Taq for PCR and T4 DNA ligase were purchased from Takara Biotechnology Co., Ltd. (Dalian). QIAprep Spin Miniprep Kit and QIAquick Gel Extraction Kit were obtained from Qiagen China Co., Ltd. (Shanghai). *E. coli* DH5α and BL21(DE3) competent cells were purchased from Tiangen Biotech Co., Ltd. (Beijing). Improved minimal essential medium (IMEM), Dulbecco's modified Eagle's medium (DMEM), fetal bovine serum (FBS), trypsin, and 1x nonessential amino acids were all from Gibco BRL, USA. Apoferritin, insulin, and EGF were obtained from Sigma Chemical Co., Ltd., China. Fluorescein-5-maleimide (FAM) was purchased from Enzo Life Sciences, Inc., USA. Alexa Fluor 750 was obtained from Invitrogen, USA. Other chemical reagents were analytical or chromatographic grade.

Cloning of Human FTH1: The gene encoding human FTH1 was amplified by PCR using a forward primer with an EcoR I site (5′-ACTgaattcATGACGACCGCGTCCACC-3′) and reverse primer with a Not I site (ACTgcggccgcTTAGCTTTCATTATCACTGT CTCC-3′) for amplification. The PCR product was subsequently cloned into the pET-28a(+) plasmid. After the plasmid vector was transformed into DH5α, positive colonies were selected by PCR using T7 primers, and were grown overnight in LB medium (3 mL) containing kanamycin (50 μg mL^{-1}). The FTH1 plasmid was isolated using a QIAprep Spin Miniprep Kit and inserted DNA was confirmed by DNA sequencing.

Cloning of Human EGF-FTH1 Fusion Gene: Human EGF gene was obtained by overlapping PCR. First, a 97 base pair (bp) PCR product was amplified using forward primer 5′-GATGGGTACTGCCTCCATGATGGTGTGTGCATGTATATTGAAGCATTGGACAAGTATGC-3′) and reverse primer 5′-GACATCGCTCCCCGATGTAGCCAACAACACAGTTGCATGCATACTTGTCCAATGCTTCA-3′. Then, the full-length EGF gene was amplified by using the above 97-bp PCR product as the template with the following primers: 5′-CATGCCATGGCAATGAATAGTGACTCTGAAT GTCCCCTGTCCCACGATGGGTACTGCCTCCATGA-3′ and 5′-CCGGAATTCGCGCAGTTCCCACCACTTCAGGTCTCGGTACTGACATCGCTCCCCG-ATGTAGC-3′ (the Nco I and EcoR I restriction sites underlined). To incorporate the EGF sequence onto the N terminus of the human FTH1, the full-length EGF PCR produced was digested with Nco I and EcoR I, and cloned into pET-28(a)/FTH1 plasmid. The plasmid was isolated and inserted DNA was confirmed by DNA sequencing.

Expression and Purification of EGF-FTH1 Nanoparticles: *E. coli* BL21(DE3) cells were transformed (by heat shock) with pET-28(a)/EGF-FTH1 plasmid and grown in LB medium containing kanamycin (50 μg mL^{-1}) at 37 °C. When the optical density reached 0.6 (600 nm), isopropyl-β-D-thiogalactoside (IPTG, 1 mM) was added to induce protein expression. After 12 h of induction at 37 °C, cells were harvested by centrifugation at 5000 *g* (20 min) and stored overnight at −20 °C. The cells were then washed once with Buffer A (50 mM Tris-HCl, pH 7.9) and disrupted by sonication. The inclusion bodies (IBs) from these cell lysates were recovered by centrifugation at 5000 *g* (4 °C, 15 min), and washed four times with Buffer B (50 mM Tris-HCl, 50 mM NaCl, 1 mM EDTA, 1% Triton X-100, pH 7.9) and twice with Buffer C (50 mM Tris-HCl, 1 mM EDTA,10 mM dithiothreitol (DTT), pH 7.9). The IBs were solubilized by incubating in Buffer C containing 8 M urea at 37 °C for 1 h and then at 25 °C overnight. The denatured protein concentration was determined by the Bradford Protein Assay and then analyzed by SDS-PAGE. Afterwards, the denatured protein was refolded at 4 °C by sequentially dialyzing against 4, 3, 2, and 0 M urea in Buffer D (50 mM Tris-HCl, 0.5 mM EDTA, 50 mM NaCl, 10% glycerol, 0.1% polyethylene glycol (PEG), 0.2 mM glutathione (reduced), 0.1 mM glutathione (oxidized), pH 7.9) and then in Buffer E (50 mM Tris-HCl, 50 mM NaCl, 10% glycerol, pH 7.9) to remove the PEG, EDTA, and glutathione. Finally, the recombinant protein was isolated by filtration and concentrated using an Amicon Ultra device.

Transmission Electron Microscopy (TEM): EGF-FTH1 nanoparticles were examined using a Joel JEM-1230 transmission electron microscope. Electron diffraction patterns were recorded from a selected area that was well occupied with EGF-FTH1 nanoparticles. Particle size was determined by measuring at least ten nanoparticles.

Labeling of EGF-FTH1 Nanoparticles: FAM or Alexa Fluor 750 was used to fluorescently label EGF-FTH1 via reaction with cysteine residues of EGF-FTH1 molecules. Briefly, EGF-FTH1 (500 μg) in PBS buffer (100 μL) was incubated with FAM (0.5 mg; or Alexa Fluor 750) at room temperature for 30 min and then overnight at 4 °C. The labeled protein was separated from free dye using a Sephadex G25 desalting column, and then quantified using absorbance spectroscopy as described in Ref. [33].

Cells and Cell Cultures: Human normal breast epithelial MCF-10A and breast carcinoma MCF-7 cell lines were originally purchased from the American Type Culture Collection (ATCC). MCF-7 cells were routinely maintained in IMEM supplemented with 10%

NANO MICRO small

FBS, 1x nonessential amino acids, 10 mM 4-(2-hydroxyethyl)-1-piperazineethanesulfonic acid (HEPES), and insulin (10 μg mL^{-1}). MCF-10A and MDA-MB-231 cells were cultured as previously described.[34]

In vitro Cytotoxicity Assay: MCF-10A, MCF-7, and MDA-MB-231 cells were subcultured in 96-well plates at a density of 1×10^3, 3×10^3, and 3×10^3 cells per well overnight, respectively. Then the cells were treated with apoferritin (6 μM), EGF (20 ng mL^{-1}), or EGF-FTH1 (6 μM) in full growth medium. Forty-eight hours later cell viability was determined by 3-(4,5-dimethylthiazol-2-yl)-2,5-diphenyltetrazolium bromide (MTT) assay.

Fluorescence-Activated Cell Sorting (FACS) Analysis: Flow cytometry was performed on a FACScalibur instrument (Becton Dickinson, Mountain View, CA) and analyzed using Cell Quest software (Becton Dickinson). In brief, 5×10^5 cells were incubated with fluorescein-labeled nanoparticles (normalized to the same concentration of fluorescein) in PBS containing 0.5% bovine serum albumin (BSA) on ice for 1 h. The cells were washed three times with 0.5% BSA in PBS and then resuspended in 0.5% BSA (0.5 mL) in PBS for FACS assays. The binding specificity of EGF-FTH1 nanoparticles to breast cancer cells was also examined in competition experiments, in which cells were incubated with fluorescein-labeled EGF-FTH1 nanoparticles in the presence of free EGF prior to FACS assays. The EC_{50} and maximum geometric mean fluorescence intensity were calculated by OriginPro 8 (OriginLab Corporation, Massachusetts).

Fluorescence Microscopy: Cells were subcultured in 24-well plates at a density of 2.2×10^5 cells per well. After 12 h, the cells were incubated with fluorescein-labeled nanoparticles in the presence or absence of 20 μM EGF. All nanoparticles were normalized to 0.5 μM fluorescein. The cells were washed twice with PBS and then visualized under a microscope (Nikon, TE2000-U).

Animal Model: All animal experiments were performed in accordance with a protocol approved by Shanghai Laboratory Animal Care and Use Committee. The MDA-MB-231 tumor model was established by subcutaneous injection of MDA-MB-231 cells (2×10^7 in a mixture of 200 μL PBS) into the front flank of ≈20 g female athymic nude mice (Balb/c). After 2 weeks, tumors reached a size of 100–300 mm^3.

In vivo Toxicity Studies: When the tumor volume had reached 100 mm^3, mice were divided into two groups of three mice, thereby minimizing weight and tumor size differences. Tumor-bearing nude mice were treated every other day by i.v. injection of EGF-FTH1 nanoparticles (1.0 nmol) or PBS for 10 days. During the dosing period, the mice were monitored for weight and tumor size daily. The tumor size was calculated by the following formula: $(\text{width}^2 \times \text{length})/2$.

In vivo Tumor Targeting Studies: The mice underwent imaging studies when the tumor volume reached 500–800 mm^3 (3–4 weeks after inoculation). Generally, EGF-FTH1 was first conjugated with Alexa Fluor 750 as described above. Then, the labeled EGF-FTH1 (0.5 nmol) in PBS (100 μL) was administered intravenously into the athymic nude mice bearing subcutaneous MDA-MB-231 tumors. Two hours later, fluorescence images were acquired on a KODAK in vivo multispectral Imaging System FX using the filter (excitation 740 nm, emission 790 nm). After that, the tumor-bearing mice were sacrificed by exsanguination, and the tumors and major organs were harvested. Each organ was rinsed with PBS three times and the tissue distribution of nanoparticles was quantified by measuring the NIR fluorescence intensity at the region of interest. All values are expressed as means ± SE for groups of three animals.

For the competitive inhibition study, Alexa Fluor 750-labeled EGF-FTH1 nanoparticles were intravenously injected into MDA-MB-231 tumor-bearing mice 30 min after i.v. administration of a high dose of EGF (0.2 mg in 100 μL PBS). The NIR fluorescence images of the whole body or major organs/tumors were taken 2 h after administration of EGF-FTH1 nanoparticles.

Statistical Analyses: Statistical analyses were performed using one-way ANOVA with Fisher's test. A p value of less than 0.05 ($p < 0.05$) was accepted as statistically significant. All data analyses were performed using PASW Statistics 18 software (SPSS Inc., Chicago, USA).

Acknowledgements

This work was supported by the National Natural Science Foundation of China (Nos. 20805015, 21010102009), the State of Nebraska LB595 Research Program (USA), the Innovation Program of Shanghai Municipal Education Commission (No. 12ZZ048), Shanghai Committee of Science and Technology (11nm0505200, 10142200803, 11142200703, 11142201200), the Fundamental Research Funds for the Central Universities (ECUST No. WF0914025), and the National Special Fund for State Key Laboratory of Bioreactor Engineering (Grant No. 2060204).

[1] A. Jemal, R. Siegel, J. Xu, E. Ward, *CA Cancer J. Clin.* **2010**, *60*, 277.
[2] N. Sanvicens, M. P. Marco, *Trends Biotechnol.* **2008**, *26*, 425.
[3] L. Y. T. Chou, K. Ming, W. C. W. Chan, *Chem. Soc. Rev.* **2011**, *40*, 233.
[4] T. Douglas, M. Young, *Science* **2006**, *312*, 873.
[5] A. MaHam, Z. W. Tang, H. Wu, J. Wang, Y. H. Lin, *Small* **2009**, *5*, 1706.
[6] E. C. Theil, *Annu. Rev. Biochem.* **1987**, *56*, 289.
[7] J. Y. Ahn, H. Choi, Y. H. Kim, K. Y. Han, J. S. Park, S. S. Han, J. Lee, *Nucleic Acids Res.* **2005**, *33*, 3751.
[8] C. R. Kaiser, M. L. Fleniken, E. Gillitzer, A. L. Harmsen, A. G. Harmsen, M. A. Jutila, T. Douglas, M. J. Young, *Int. J. Nanomed.* **2007**, *2*, 715.
[9] M. Uchida, M. L. Flenniken, M. Allen, D. A. Willits, B. E. Crowley, S. Brumfield, A. F. Willis, L. Jackiw, M. Jutila, M. J. Young, T. Douglas, *J. Am. Chem. Soc.* **2006**, *128*, 16626.
[10] N. Stephanopoulos, G. J. Tong, S. C. Hsiao, M. B. Francis, *ACS Nano* **2010**, *4*, 6014.
[11] F. M. Brunel, J. D. Lewis, G. Destito, N. F. Steinmetz, M. Manchester, H. Stuhlmann, P. E. Dawson, *Nano Lett.* **2010**, *10*, 1093.
[12] G. J. Tong, S. C. Hsiao, Z. M. Carrico, M. B. Francis, *J. Am. Chem. Soc.* **2009**, *131*, 11174.
[13] G. Destito, R. Yeh, C. S. Rae, M. G. Finn, *Chem. Biol.* **2007**, *14*, 1152.
[14] P. A. Suci, S. Kang, M. Young, T. Douglas, *J. Am. Chem. Soc.* **2009**, *131*, 9164.
[15] Y. Ren, S. M. Wong, L. Y. Lim, *Bioconjugate Chem.* **2007**, *18*, 836.
[16] X. Lin, J. Xie, G. Niu, F. Zhang, H. Gao, M. Yang, Q. Quan, M. A. Aronova, G. Zhang, S. Lee, R. Leapman, X. Chen, *Nano Lett.* **2011**, *11*, 814.
[17] S. Tsutsui, S. Ohno, S. Murakami, Y. Hachitanda, S. Oda, *Breast Cancer Res. Treat.* **2002**, *71*, 67.

[18] A. Gschwind, O. M. Fischer, A. Ullrich, *Nat. Rev. Cancer* **2004**, *4*, 361.
[19] Z. Yang, X. Wang, H. Diao, J. Zhang, H. Li, H. Sun, Z. Guo, *Chem. Commun.* **2007**, 3453.
[20] A. Lostumbo, D. Mehta, S. Setty, R. Nunez, *Exp. Mol. Pathol.* **2006**, *80*, 46.
[21] S. M. Singh, A. K. Panda, *J. Biosci. Bioeng.* **2005**, *99*, 303.
[22] L. Li, C. J. Fang, J. C. Ryan, E. C. Niemib, J. A. Lebrónc, P. J. Björkman, H. Arase, F. M. Torti, S. V. Torti, M. C. Nakamura, W. E. Seaman, *Proc. Natl. Acad. Sci. USA* **2010**, *107*, 3505.
[23] M. Terashima, M. Uchida, H. Kosuge, P. S. Tsao, M. J. Young, S. M. Conolly, T. Douglas, M. V. McConnell, *Biomaterials* **2011**, *32*, 1430.
[24] C. Mamot, D. C. Drummond, U. Greiser, K. Hong, D. B. Kirpotin, J. D. Marks, J. W. Park, *Cancer Res.* **2003**, *63*, 3154.
[25] L. Yang, H. Mao, Y. A. Wang, Z. Cao, X. Peng, X. Wang, H. Duan, C. Ni, Q. Yuan, G. Adams, M. Q. Smith, W. C. Wood, X. Gao, S. Nie, *Small* **2009**, *5*, 235.
[26] C. Park, H. Youn, H. Kim, T. Noh, Y. H. Kook, E. X. Oh, H. J. Park, C. Kim, *J. Mater. Chem.* **2009**, *19*, 2310.
[27] X. Montet, M. Funovics, K. M. Abou, R. Weissleder, L. Josephson, *J. Med. Chem.* **2006**, *49*, 6087.
[28] S. Hong, P. R. Leroueil, I. J. Majoros, B. G. Orr, J. R. Baker, M. M. B. Holl, *Chem. Biol.* **2007**, *14*, 107.
[29] D. B. Kirpotin, D. C. Drummond, Y. Shao, M. R. Shalaby, K. Hong, U. B. Nielsen, J. D. Marks, C. C. Benz, J. W. Park, *Cancer Res.* **2006**, *66*, 6732.
[30] D. E. Prasuhn, P. Singh, E. Strable, S. Brown, M. Manchester, M. G. Finn, *J. Am. Chem. Soc.* **2008**, *130*, 1328.
[31] C. H. J. Choi, C. A. Alabi, P. Webster, M. E. Davis, *Proc. Natl. Acad. Sci. USA* **2010**, *107*, 1235.
[32] Z. Zhang, J. Chen, L. Ding, H. Jin, J. F. Lovell, I. R. Corbin, W. Cao, P. Lo, M. Yang, M. Tsao, Q. Luo, G. Zheng, *Small* **2010**, *6*, 430.
[33] M. L. Flenniken, D. A. Willits, S. Brumfield, M. Young, T. Douglas, *Nano Lett.* **2003**, *3*, 1573.
[34] Y. Xie, D. W. Wolff, T. Wei, B. Wang, C. Deng, J. K. Kirui, H. Jiang, J. Qin, P. W. Abel, Y. Tu, *Cancer Res.* **2009**, *69*, 5743.

Received: January 11, 2012
Published online: May 23, 2012

